American Mineralogist, Volume 87, pages 1183–1189, 2002

Structure change of $Ca_{1-x}Sr_xTiO_3$ perovskite with composition and pressure

TAKAMITSU YAMANAKA,* NORIYUKI HIRAI, AND YUTAKA KOMATSU

Department of Earth and Space Science, Graduate School of Science, Osaka University, 1-1, Machikaneyama Toyonaka Osaka, 560-0043 Japan

ABSTRACT

Structure refinements of solid solutions of $(Ca_{1-x}Sr_x)TiO_3$ (x = 0.0, 0.25, 0.5, 0.6, 0.65, and 1.0) were undertaken using single crystals at ambient conditions. Their lattice constants, *c/a* axial ratios, and cell volumes indicate continuous changes from orthorhombic to cubic through a tetragonal phase. The orthorhombic structure is continuous between x = 0.0 and x = 0.6, and a phase at x = 0.65 shows a tetragonal structure with space group *I*4/*mcm*. With increasing Sr substitution, the symmetry changes to cubic with $Pm\bar{3}m$ space group. A-O and B-O distances in ABO_3 perovskite were determined as a function of the composition of the A cation (Ca and Sr). Tilting and rotation angles of the TiO_6 octahedral linkage with x of $(Ca_{1-x}Sr_x)TiO_3$ were also evaluated. Single-crystal structure refinements of $Ca_{0.35}Sr_{0.65}TiO_3$ perovskite at 3.5, 4.1, and 7.0 GPa at 300 K were carried out using a diamond anvil cell. The tetragonal phase transforms to an orthorhombic structure with space group *Pbnm* at 3.5 GPa. The polymorphic transition of $^{VIII}A^{2+VI}B^{4+}O_3$ perovskites under compression is discussed.

INTRODUCTION

The silicate perovskites are dominant silicate phases in mineral assemblages of the Earth's lower mantle. Numerous high-pressure experiments using diamond anvil cells or multianvil equipment have been carried out in order to understand the phase stabilities and isothermal compression of various silicates together with analogous materials such as germanate and titanate perovskites. Many X-ray diffraction studies on magnesium and iron silicate perovskites [$(MgFe)SiO_3$] have been reported. Calcium silicates also play an important role in phase relations and elasticity of the lower mantle, hence much attention has been paid to calcium-bearing silicate perovskites. The equation of state (EOS) of $CaSiO_3$ perovskite was determined by diamond anvil cell (DAC) experiments with YAG laser heating up to 134 GPa (Mao et al. 1989). The EOS, thermal expansion, and elastic properties of $CaSiO_3$ have also been determined with DAC or multianvil presses (Yagi et al. 1989; Wang et al. 1996; Shim et al. 2000a, 2000b).

The structure of $MgSiO_3$ perovskite has been analyzed using quenched samples (Horiuchi et al. 1987). However, the detailed structure of $CaSiO_3$ perovskite cannot be studied because the phase is not quenchable to ambient conditions. Consequently, the precise symmetry and details of the structural transition remain undetermined.

The structures of $CaTiO_3$ and $CaGeO_3$, possible analogues of $CaSiO_3$, were studied by Sasaki et al. (1987). Structural changes in $CaTiO_3$ were intensively investigated at elevated temperature under ambient pressure (Redfern 1996; Liu and Liebermann 1993; Kennedy et al. 1999), and a series of thermal transitions [orthorhombic (*Pbnm*) → tetragonal (*I*4/*mcm*) → cubic ($Pm\bar{3}m$)] was proposed with increasing temperature.

Bednorz and Muller (1984) measured the temperature dependence of the dielectric constant in the range $x > 0.88$ for $(Ca_{1-x}Sr_x)TiO_3$ from 4 to 300 K and found that the dielectric nature decreases rapidly with substitution of Sr^{2+} by Ca^{2+} because of internal lattice distortion. Ranjan et al. (1999) used neutron and X-ray powder diffraction to study $(Sr_{1-x}Ca_x)TiO_3$ with $x > 0.12$ at high temperatures and found that it was orthorhombic; in addition, an intermediate phase between orthorhombic and cubic was found in the range of $0.12 < x < 0.21$. The cubic-tetragonal transition of $SrTiO_3$ was studied using Landau theory by Hayward and Salje (1999) and Salje (1998). Carpenter et al. (2001) performed a strain analysis of the phase transition in $(Ca,Sr)TiO_3$ perovskite.

Xiong et al. (1986) used X-ray powder diffraction to study high-pressure transformations in orthorhombic $CaTiO_3$. They found that orthorhombic $CaTiO_3$ (I) transforms to hexagonal perovskite (II) at about 10 GPa at room temperature and that at 1000 °C the orthorhombic phase first transforms into a tetragonal (III) phase at 8.5 GPa and then to a hexagonal (II') form at 15 GPa under nonhydrostatic conditions. However, Ross and Angel (1999) found no phase transition in their single-crystal diffraction study up to 10 GPa.

Structural discussions of $(Ca_{1-x}Sr_x)TiO_3$ can be applied to the crystal chemistry of the $(Mg_{1-x}Fe_x)SiO_3$ perovskite solid solution. It is known that $SrTiO_3$, an end-member of the solid solution, has the cubic perovskite structure at room condition, and that the other end-member ($CaTiO_3$) is orthorhombic. Accordingly, solid solutions of $(Ca_{1-x}Sr_x)TiO_3$ change symmetry (from orthorhombic to cubic) with increasing x. In the present experiment, structure change as a function of the cation ratio (x) at the A site and structure change at high-pressure were investigated by single-crystal structure analysis. Cation ordering in the ABO_3 perovskite structure was also examined at high pressure. Leinenweber et al. (1997) used electron diffraction

* E-mail: b61400@center.osaka-u.ac.jp

to study structural variations in the solid solution $Ca(Ti_xSi_{1-x})O_3$ and found a cation-ordered structure of Ca_2TiSiO_6 with space group symmetry of $Fm\bar{3}m$.

EXPERIMENTAL METHODS

Sample preparation

Single crystals of the solid solutions of $(Ca_{1-x}Sr_x)TiO_3$ (x = 0.0, 0.2, 0.5, 0.6, 0.65, and 1.0) were synthesized for X-ray structure analyses. Powder mixtures of the end-members $CaTiO_3$ and $SrTiO_3$ were heated with TiO_2 flux at 1650 °C for 24 hours and then the temperature was gradually decreased by 5 °C/hour to 1500 °C. The product was transparent platy crystals with maximum size of 1000 × 400 × 500 μm.

Homogeneity and chemical impurities in the synthesized crystals were examined by EPMA and no trace elements were found. The crystallinity was tested by optical microscope and X-ray precession photography.

X-ray diffraction study at ambient conditions

Approximately cube-shaped crystals were selected for X-ray diffraction experiments at ambient conditions. Spherical specimens about 200 μm in diameter were prepared by Bond's method. Intensity measurements were made with a four-circle diffractometer (RIGAKU AFC-5 and AFC-6) using Mo$K\alpha$ radiation (λ = 0.71069 Å) emitted from a rotating anode X-ray generator (50 kV, 180 mA) with a graphite monochromator. The ω-2θ scan mode and scan speed of 2°/min were adopted in the 2θ range of 5–120°. Reflections with $F(hkl) > 3\sigma F(hkl)$ were used for the refinement. The diffraction intensities were corrected for X-ray absorption, Lorentz, and polarization factors.

High-pressure diffraction study

A single-crystal structure analysis of $(Ca_{0.35}Sr_{0.65})TiO_3$ at 7.0 GPa was carried out using synchrotron radiation at the Photon Factory at Tsukuba. The experiments at 0.0001, 3.5, and 4.1 GPa were undertaken using Mo$K\alpha$ and Ag$K\alpha$ rotating anode X-ray generators at 50 kV and 180 mA. A diamond anvil cell (DAC) with culet sizes of 400 μm was used to generate high pressures. A single crystal 40 × 60 μm wide and 20 μm thick was placed in the gasket hole (200 μm in diameter) and a Be hemisphere was used as a backing plate. Ruby chips (pressure markers) and a pressure transmitting medium with methanol:ethanol:H_2O = 16:3:1 were also kept in the hole. Hydrostatic conditions could be guaranteed within the present pressure range. A spring steel gasket was preindented to 80 μm in thickness. Pressure measurement was made by means of the ruby fluorescence system. The pressure was measured before and after each diffraction measurement. The pressure difference between the two measurements was within 5%. Sample centering on the goniometer was made by the profile checking method using the direct beam. This method placed the sample in the center with an accuracy of 20 μm.

Diffraction intensity data were collected with the ω-scan mode (ϕ-fixed) with a scan speed of 1°/min, a scan width of 2° in ω, and a step interval of 0.01°/step. Reflections observed up to 2θ = 52° and with intensities of $F_o > 3\sigma(F_o)$ were used for the least-squares refinements. Details of a new system for high-pressure diffractometry and measurement are given in Yamanaka et al. (2001)

Structure change of $Ca_{1-x}Sr_xTiO_3$ with Sr substitution

Lattice constant change. The lattice constants were determined from the peak refinements of 15–25 reflections in the range of 40° < 2θ < 50° at ambient pressure. The lattice constants, c/a, and unit-cell volumes of the solid solutions of $(Ca_{1-x}Sr_x)TiO_3$ are presented in Table 1. The orthorhombic lattice constants are continuous between x = 0.0 and x = 0.6. In this region a and b approach the same value and at x = 0.65 a equals b, which indicates a tetragonal lattice. The lattice constants for tetragonal and cubic structures in Table 1 are converted to the orthorhombic lattice to facilitate comparison with the whole solid solution range. The value of $c = \sqrt{2}\bar{a}$, where $\bar{a}$ is an average of a and b, which indicates a deformation from the cubic perovskite, is also shown in Table 1. No abrupt change was found in the lattice constants. The lattice constants change continuously but not linearly with increasing x, as shown in Figure 1. The non-linearity implies that they are affected not only by the site volume expansion due to the substitution of Ca by Sr at the A site, but also by the TiO_6 octahedral linkage, because the lattice constants are also controlled by rotation around **c** and tilting relative to the (001) plane.

Structure refinement. The atomic scattering factors of Ca^{2+}, Sr^{2+}, and Ti^{4+} were adopted from a Hartree-Fock approximation presented in the *International Tables for X-ray Crystallography* (Wilson 1992) and are based on the fully ionized model. The scattering factor for O^{2-} was from Tokonami (1965). The full-matrix least-squares refinements were executed using the program RADY (Sasaki et al. 1987) and included the isotropic extinction parameter Gex based on crystalline mosaicity. Anharmonic thermal vibration of atoms is believed to be negligibly small at room temperature, because the present samples have quite high Debye temperatures. Consequently, we did not apply higher than second-rank thermal parameters. The refinements were carried out by minimizing the function $\Sigma(|F_{obs}| - |F_{cal}|)^2$. The converged atomic coordinates (xyz) and tempera-

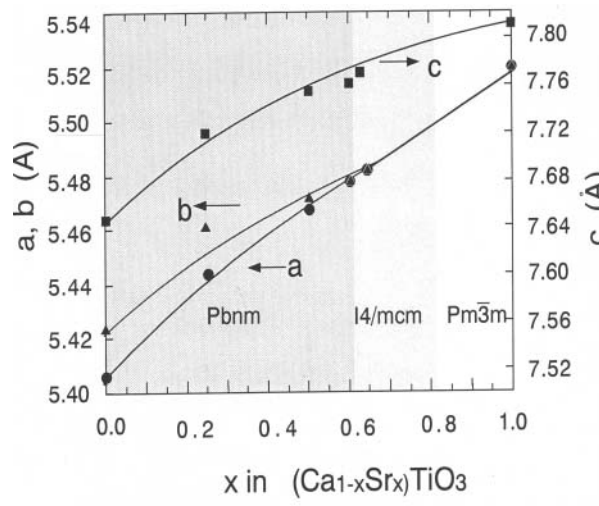

FIGURE 1. The lattice constants of the solid solutions of $(Ca_{1-x}Sr_x)TiO_3$ (x = 0.0, 0.25, 0.5, 0.6, 0.65, and 1.0).

TABLE 1. Lattice constants and structure parameters of the solid solutions of $(Ca_{1-x}Srx)TiO_3$

x		0.00	0.25	0.50	0.60	0.65	1.00
Space group		*Pbnm*	*Pbnm*	*Pbnm*	*Pbnm*	*I*4/*mcm*	*Pm*$\bar{3}$*m*
				Lattice constant			
a (Å)		5.4043(8)	5.4440(8)	5.4677(9)	5.4784(10)	5.4801(7)	5.5202(7)
b (Å)		5.4224(7)	5.4591(8)	5.4713(7)	5.4791(8)	5.4801(7)	5.5202(7)
c (Å)		7.6510(12)	7.7213(11)	7.7390(10)	7.7517(13)	7.7619(10)	7.8067(9)
c /$\sqrt{2}\bar{a}$		0.999	1.001	1.001	1.000	1.001	1.000
Cell volume(Å^3)		224.19	229.47	231.52	232.68	233.10	237.89
				Structure refinement			
Size (μm)		100 × 80 × 80	80 × 80 × 60	100 × 100 × 80	80 × 60 × 50	80 × 60 × 60	80 × 80 × 80
No. observed ref.		385	311	444	396	249	228
No. used ref.		124	111	182	145	90	164
R		0.0372	0.0376	0.0295	0.0298	0.0297	0.0346
wR		0.0313	0.0367	0.0415	0.0415	0.0348	0.0396
A(Ca,Sr)	*x*	0.9916(6)	0.9942(9)	0.9971(7)	0.9975(9)	0.0	0.0
	y	0.0123(7)	0.0090(12)	0.0080(7)	0.0053(9)	0.5	0.0
	z	0.25	0.25	0.25	0.25	0.25	0.25
	B (iso)	0.62(7)	0.88(9)	0.77(19)	0.74(5)	0.65(8)	0.48(5)
B (Ti)	*x*	0.5	0.5	0.5	0.5	0.0	0.5
	y	0.0	0.0	0.0	0.0	0.0	0.0
	z	0.0	0.0	0.0	0.0	0.0	0.0
	B (iso)	0.45(5)	0.28(8)	0.72(4)	0.82(6)	0.66(1)	0.40(6)
01	*x*	0.0586(10)	0.035(2)	0.025(2)	0.005(2)	0.0	0.0
	y	0.4687(9)	0.483(3)	0.496(2)	0.496(3)	0.0	0.5
	z	0.25	0.25	0.25	0.25	0.25	0.25
	B (iso)	1.2(2)	1.16(32)	1.2(5)	1.5(9)	1.6(4)	1.3(2)
02	*x*	0.713(1)	0.721(2)	0.730(3)	0.739(3)	0.776(1)	0.75
	y	0.288(1)	0.281(3)	0.269(3)	0.262(3)	0.276(1)	0.25
	z	0.0371(6)	0.031(2)	0.025(1)	0.022(2)	0.0	0.0
	B (iso)	1.3(3)	2.3(4)	1.8(8)	1.6(2)	1.7(3)	1.6(3)

Notes: $\bar{a}$ is a mean value of *a* and *b*. All lattice constants are normalized to the orthorhombic lattice. The refinements of x = 0.65 and x = 1.00 were undertaken with constraints of tetragonal and cubic symmetry, respectively, but their lattice constants and atomic coordinates are converted to the orthorhombic symmetry.

ture factors *B*(iso) for all solid solutions are shown in Table 1. The *R*-values ($R = w\Sigma||F_{obs}| - |F_{cal}||/\Sigma|F_{obs}|$) of the least-squares refinements are also given in Table 1. All *R*-factors converged to within $R = 0.05$.

Tetragonal phase of $Ca_{0.35}Sr_{0.65}TiO_3$. The $Ca_{0.35}Sr_{0.65}TiO_3$ phase shows tetragonal symmetry. Space group symmetries of *I*4/*mcm*, *I*$\bar{4}$*c*2, and *I*4*cm* yield the same extinction conditions: $k = 2n$ and $l = 2n$ for 0*kl* reflections. Those of *I*4/*m*, *I*$\bar{4}$2*m*, and *I*422 result in the following extinction conditions: $k + l = 2n$ for 0*kl* reflections. The validity of these space groups was examined by refining the structures. Five of them are subgroups of *I*4/*mcm*. Only *I*4/*mcm* and *I*4/*m* are centrosymmetric. The differences between the atomic coordinates for the centrosymmetric and non-centrosymmetric structures were very small. The *I*4/*mcm* space group is the most probable for the tetragonal phase $Ca_{0.35}Sr_{0.65}TiO_3$ because the model gave the lowest *R* factor ($R = 0.027$, $wR = 0.0348$) and because the temperature factors of all atoms and the bond lengths obtained from the refinement are appropriate for the perovskite structure. Other models did not produce credible structure parameters or temperature factors. Hence *I*4/*mcm* is the most probable symmetry. The converged structure parameters are presented in Table 1.

Bond lengths and bond angles for $Ca_{1-x}Sr_xTiO_3$. The tetragonal phase of $Ca_{0.35}Sr_{0.65}TiO_3$ is stable under ambient conditions. With increasing Sr substitution, the solid solution changes space group from tetragonal (*I*4/*mcm*) to cubic (*Pm*$\bar{3}$*m*). Accordingly, the tetragonal phase may exist as an intermediate structure between the orthorhombic and cubic structures in the $Ca_{1-x}Sr_xTiO_3$ solid solution.

Previous studies have shown that $CaTiO_3$ orthorhombic perovskite is characterized by an enormous deformation from the cubic symmetry. The present single-crystal structure refinements of $Ca_{1-x}Sr_xTiO_3$ revealed that the A cation in ABO_3 is surrounded by 12 neighboring O atoms at distances ranging from 2.55 to 3.1 Å. Bond lengths and selected bond angles of all samples are presented in Table 2. Four of the twelve A-O bonds longer than 2.8 Å become shorter with increasing *x* in spite of the replacement by Sr having a large ionic radius. The other eight A-O bond lengths shorter than 2.8 Å become longer. The mean $\overline{A\text{-}O}$ distance increases almost linearly from $CaTiO_3$ to $SrTiO_3$, as shown in Figure 2.

The TiO_6 octahedra deforms from the regular form. The bond angle ∠ Ti-O1-Ti is the tilting angle (θ) of the octahedron relative to (001) plane and ∠ Ti-O2-Ti is the rotation angle (ψ) around the *c* axis. The θ-angle becomes larger from 158.72° of $CaTiO_3$ with Sr substitution and approaches 180° for the tetragonal phase of $Ca_{0.35}Sr_{0.65}TiO_3$. The ψ–angle gradually increases from 156.30° for $CaTiO_3$ and ψ = 168.10° for tetragonal $Ca_{0.35}Sr_{0.65}TiO_3$. Finally, the ψ–angle reaches 180° for the cubic phase. As seen in Figure 3, the φ and ψ angles do not show the same variation with compositional change. The tilting angle is mainly derived from the *z*-coordinate of O2 (0, 0, *z*), as the orthorhombic perovskite approaches the transition to tetragonal symmetry, while the TiO_6 rotation affects the transition only a little. After the transition to tetragonal the rotation angle defined by the *x* and *y* coordinates of O1 (*x*, *y*, 0.25) changes the phase to cubic. These features are consistent with the changes in A-O1 and A-O2 given in Table 2 and the temperature factors shown in Table 1. In the orthorhombic perovskite, tilting of the octahedra induces a large shortening of two long A-O1 dis-

TABLE 2. Bond length and bond angle of $(Ca_{1-x}Srx)TiO_3$

x	0.00	0.25	0.50	0.60	0.65	1.00
space group	*Pbnm*	*Pbnm*	*Pbnm*	*Pbnm*	*I4/mnm*	*Pm3̄m*
A-O1 ×1	2.442(5)	2.570(4)	2.612(5)	2.687(4)	2.740(3)	2.760(1)
O1 ×1	2.501(5)	2.598(4)	2.676(5)	2.728(4)	2.740(3)	2.760(1)
O1 ×1	2.970(5)	2.879(4)	2.805(4)	2.752(4)	2.740(3)	2.760(1)
O1 ×1	2.983(5)	2.882(4)	2.857(5)	2.792(4)	2.740(3)	2.760(1)
O2 ×2	2.317(3)	2.404(3)	2.505(3)	2.565(3)	2.603(2)	2.760(1)
O2 ×2	2.672(3)	2.695(3)	2.684(3)	2.668(3)	2.603(2)	2.760(1)
O2 ×2	2.728(3)	2.750(3)	2.764(3)	2.795(3)	2.887(3)	2.760(1)
O2 ×2	3.164((3)	3.102(3)	3.013(3)	2.945(3)	2.889(2)	2.760(1)
Mean(8)	2.547(3)	2.608(3)	2.649(3)	2.684(3)	2.709(2)	2.760(1)
Mean(12)	2.721(3)	2.736(3)	2.740(3)	2.742(3)	2.744(2)	2.760(1)
A-O(4-long)	3.070(4)	2.991(3)	2.922(4)	2.859(3)	2.814(3)	2.760(1)
B-01 ×2	1.946(1)	1.942(4)	1.940(5)	1.938(1)	1.941(2)	1.952(1)
02 ×2	1.951(3)	1.949(3)	1.953(3)	1.942(2)	1.948(2)	1.952(1)
02 ×2	1.960(3)	1.963(3)	1.947(3)	1.951(2)	1.948(2)	1.952(1)
Mean(6)	1.952(2)	1.951(2)	1.947(2)	1.944(2)	1.946(2)	1.952(1)
∠Ti-01-Ti	158.72	167.64	171.73	177.94	180.00	180.00
∠Ti-02-Ti	156.30	160.37	165.25	168.70	168.10	180.00
$V(TiO_6)$	9.90(4)	9.87(4)	9.81(4)	9.73(4)	9.82(3)	9.91(1)
			Tolerance factor			
AO(8)/ √2 BO	0.9225	0.9452	0.9622	0.9764	0.9845	1.0000
AO(12)/ √2 BO	0.9856	0.9884	0.9953	0.9977	0.9973	1.0000

Notes: Tolerance factors are not from $t = (r_A+r_O)/\sqrt{2}\,(r_B+r_O)$ but given by the observed bond length. The terms of mean(8) and mean(12) indicates an average value of eight short bond lengths and all 12 bond lengths, respectively.

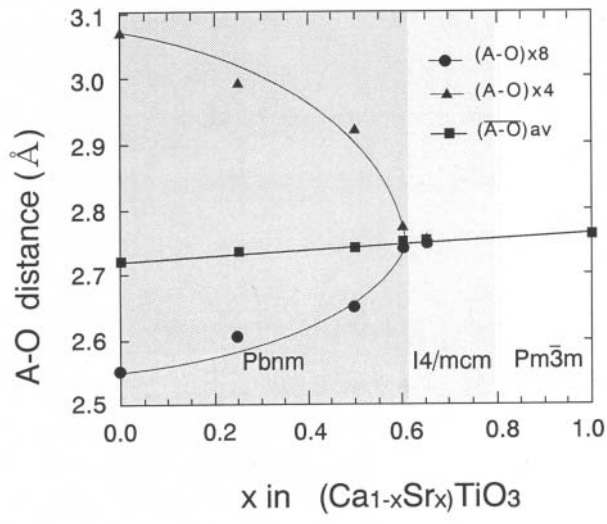

FIGURE 2. Variation of A-O distance with *x*.

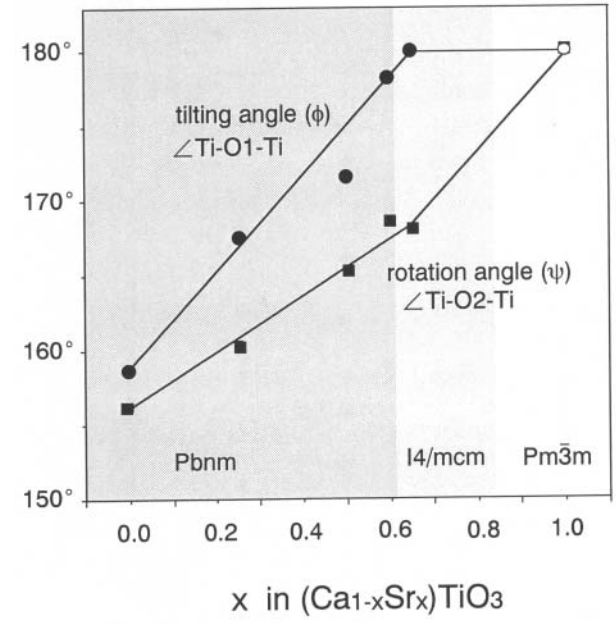

FIGURE 3. The tilting angle (ϕ) and rotation angle (ψ) of octahedral linkage.

tances, and rotation shortens the two long A-O2 distances, even in the tetragonal phase. *B*(iso) of O1 increases with Sr substitution in the orthorhombic phases. This positional disorder is attributed to the TiO_6 tilting, while *B*(iso) of O2 becomes small. *B*(iso) values of both O atoms become smaller after the transition to tetragonal resulting in the lessening of the positional disorder of O atoms.

The mean $\overline{B\text{-}O}$ distance is slightly decreased in the orthorhombic region with *x* increasing up to 0.60, as the ϕ angle increases up to 180°. However, the $\overline{B\text{-}O}$ distance becomes larger in the tetragonal and cubic regions where $x > 0.65$ (Fig. 4). The TiO_6 (same as BO6) octahedron approaches a regular shape as ψ is further increased to 180°. The TiO_6 octahedral volume does not show a linear increase (again, same as $\overline{B\text{-}O}$).

Structure transition of the tetragonal phase of $Ca_{0.35}Sr_{0.65}TiO_3$ under compression

High-pressure structure investigation of the tetragonal phase of $Ca_{0.35}Sr_{0.65}TiO_3$ was undertaken at room temperature and at pressures of 0.0001, 3.5, 4.1, and 7.0 GPa. All diffraction measurements were carried out using the single crystals and the DAC. Lattice constants at 3.5 and 4.1 GPa were determined with the Ag*K*α rotating anode X-ray generator (55 kV, 150 mA) and those at 7.0 GPa were measured with synchrotron radia-

TABLE 3. Experiment condition and lattice constant of $(Ca_{0.35}Sr_{0.65})TiO_3$ under compression

Pressure (GPa)	0.0001	3.5	4.1	7.0
Space group	*I*4/*mcm*	*Pbnm*	*Pbnm*	*Pbnm*
X-ray	Mo*K*α	Ag*K*α		PF (BL10A)
Wave length	0.71069 Å	0.56083 Å		0.41625 Å
Compression	DAC	DAC		DAC
Crystal size (μm)	80 × 60 × 50	80 × 60 × 50		60 × 80 × 40
Temperature	300 K	300 K		300 K
Spacial regeon (2θ)	<60	<60		<55
sinθ/λ	>0.704	>0.891		>1.1093
a (Å)	5.473(6)	5.456(9)	5.423(9)	5.415(7)
b (Å)	5.473(6)	5.472(9)	5.420(9)	5.412(7)
c (Å)	7.742(9)	7.688(13)	7.647(12)	7.637(9)
$c/\sqrt{2}a$	1.000	0.995	0.997	0.997
Cell volume(Å^3)	231.9	229.5	224.8	223.8

Note: The lattice constants of tetragonal phase are converted to the orthorhombic symmetry.

tion at the Photon Factory KEK at Tsukuba. The experimental conditions and the observed lattice constants at pressures of 0.0001, 3.5, 4.1, and 7.0 GPa are shown in Table 3. The sample kept in the DAC at 0.0001 GPa was probably somewhat compressed and the lattice constants and refined structure data are slightly different from those for 0.0001 GPa presented in Table 1 and 2.

The single-crystal diffraction study showed that the tetragonal phase transformed to the orthorhombic phase at 3.5 GPa. The possible orthorhombic structure at 7.0 GPa and 300 K has a subgroup symmetry of I4/*mcm*. Probable candidates *Pbnm*, $Pb2_1m$, $P2_1nm$, and $Pbn2_1$ were generated from *I*4/*mcm*, e.g., through the following path: $I4/mcm \rightarrow P4_2/mbc \rightarrow Pbam \rightarrow Pbnm\ (Pnma) \rightarrow Pb2_1m$ (or $P2_1nm$ or $Pbn2_1$). The extinction conditions for these space groups are different, but the diffraction intensities under high pressures are often too weak to allow unambiguous identification of the proper symmetry. Intensity measurement using the DAC is difficult because of the blind region and absorption resulting from the DAC geometry.

Structures were refined for all four-space groups. It was evident from the *R*-factors that the most reliable structure has *Pbnm* symmetry. The results of the structure refinements at 0.0001, 4.1, and 7.0 GPa are presented in Table 4 and the bond lengths at each pressure are shown in Table 5.

The present experiment concludes the symmetry descent from a tetragonal phase to an orthorhombic phase at high pressures. Deformation under compression generates the rotation and tilting motion of TiO_6 octahedral linkage and the rotation ψ and tilting ϕ angle become smaller, because the different volume compressions of the A and B cation sites do not result in a homogeneous compression of the unit cell.

DISCUSSION

The change in symmetry with Sr substitution is necessarily related to the relative volume expansions of the cation polyhedra. The larger ϕ and ψ angles of octahedral linkage with increasing substitution reduces the deformation of the polyhedra, as the observed tolerance factor t ($=\overline{A\text{-}O}/\sqrt{2}\overline{B\text{-}O}$) increases, as shown in Table 2. The polyhedra enhance the site symmetries from those of the orthorhombic perovskite to tetragonal and further to cubic.

TABLE 4. Structure refinement of $(Ca_{0.35}Sr_{0.65})TiO_3$ under compression

Pressure (GPa)		0.0001	4.1	7.0
Observed ref.		158	123	184
Independent ref.		92	64	83
R		0.0325	0.0683	0.0544
wR		0.0355	0.0749	0.0535
A1 (Ca,Sr)	x	0.0	0.969(2)	0.988(1)
	y	0.5	0.024(2)	0.012(1)
	z	0.25	0.25	0.25
	B(iso)	0.42(4)	0.76(8)	0.22(4)
B (Ti)	x	0.0	0.0	0.0
	y	0.0	0.5	0.5
	z	0.0	0.0	0.0
	B(iso)	0.52(5)	0.62(9)	0.51(6)
O1	x	0.0	0.035(1)	0.036(9)
	y	0.0	0.527(5)	0.543(11)
	z	0.25	0.25	0.25
	B(iso)	1.49(49)	1.43(81)	2.20(68)
O2	x	0.768(3)	0.765(7)	0.768(4)
	y	0.264(2)	0.243(6)	0.233(7)
	z	0.0	0.011(2)	0.010(6)
	B(iso)	1.32(24)	1.32(45)	0.75(15)

TABLE 5. Bond length of $(Ca_{0.35}Sr_{0.65})TiO_3$ under compression

Pressure (GPa)	0.0001	4.1	7.0
Space group	I4/mcm	Pbnm	Pbnm
A-O1 ×1	2.737(3)	2.69(1)	2.55(1)
O1 ×1	2.737(3)	2.72(3)	2.59(5)
O1 ×1	2.737(3)	2.73(1)	2.84(5)
O1 ×1	2.737(3)	2.74(3)	2.88(1)
O2 ×2	2.651(9)	2.44(3)	2.45(4)
O2 ×2	2.651(9)	2.70(3)	2.73(4)
O2 ×2	2.826(9)	2.85(3)	2.75(4)
O2 ×2	2.826(9)	2.85(3)	2.85(4)
Mean(8)	2.694(8)	2.67(3)	2.63(4)
Mean(12)	2.738(7)	2.71(3)	2.71(4)
B-O1 ×2	1.936(2)	1.923(3)	1.933(6)
O2 ×2	1.92(1)	1.89(3)	1.92(3)
O2 ×2	1.92(1)	1.95(4)	1.92(3)
Mean (6)	1.93(1)	1.92(2)	1.92(2)
Tolerance factor			
AO(8)/√2BO	0.9880	0.9843	0.9687
AO(12)/√2BO	1.0042	0.9990	0.9956

Notes: Tolerance factors are not from $t = (r_A+r_O)/\sqrt{2}(r_B+r_O)$ but given by the observed bond length. The terms of mean(8) and mean(12) indicates an average value of eight short bond lengths and all 12 bond lengths, respectively.

The tilting angle ϕ of the octahedra relative to the (001) plane and the rotation ψ around the **c** axis becomes greater with Sr substitution. This generates fourfold rotation along **c**, resulting in the transition from the *Pbnm* orthorhombic structure to *I*4/*mcm* tetragonal perovskite. Both the tilting angle ∠Ti-O1-Ti and the rotation angle ∠Ti-O2-Ti become 180°. The octahedron has the ideal tetragonal site symmetry of 4/*mmm* and, finally, the perovskite transforms to the cubic structure of $Pm\bar{3}m$ (Fig. 5).

Possible structures derived from cubic perovskite ($Pm\bar{3}m$) have been proposed on the basis of the rotation and tilting of octahedral linkages by group-theoretical analysis (Glazer 1972; Howard and Stokes 1998). Our single-crystal structure refinements of the $Ca_{1-x}Sr_xTiO_3$ solid solutions show that positional disorder of the O atoms provides the motivation for the structure change. The temperature factors for O1 and O2 show strong anisotropy and cause enhancement of the tilting and rotation of the octahedral-linkage with increasing Sr substitution in the

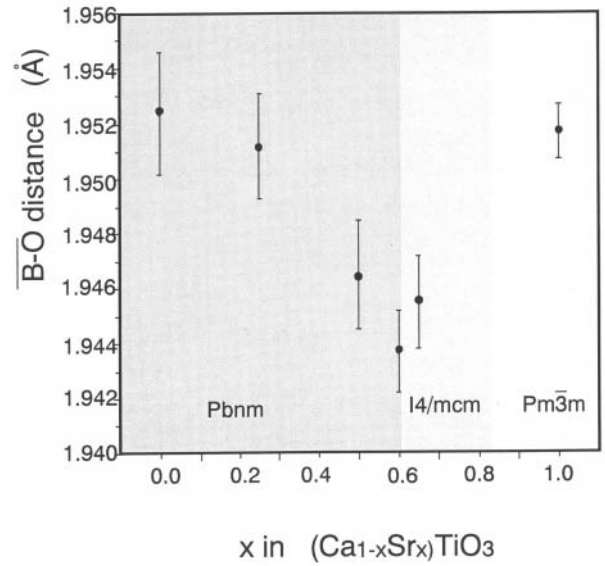

FIGURE 4. Variation of the average $\overline{B\text{-}O}$ distance with x.

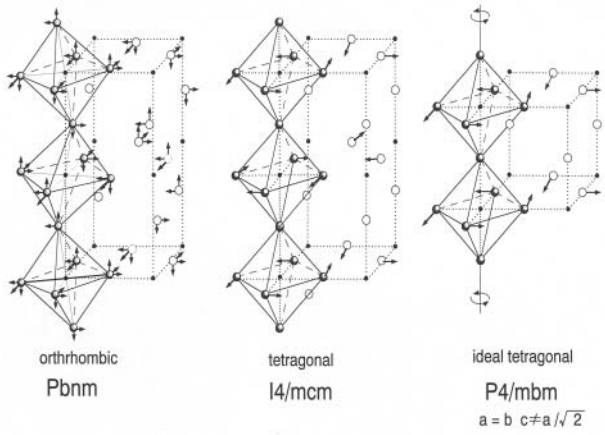

FIGURE 5. Possible high-pressure polymorphs of $(Ca_{1-x}Sr_x)TiO_3$ perovskite. The octahedral linkages and atomic positional displacements of O1 and O2 show strong anisotropy. The arrows indicate the directions of freedom of atomic vibration.

orthorhombic region, as shown in Figure 5. B_{iso} of O2 is larger than that of O1, which probably indicates a greater degree of rotation of the TiO_6 octahedra in comparison with the tilting motion. With increasing Sr substitution, the tilting of the octahedra decreases, as indicated by atomic positions and temperature factors for O1. Then the coplanar O2 atoms are related by a fourfold rotation, inducing the transformation from orthorhombic to tetragonal perovskite. The expansion of the unit-cell volume results from increasing size of cations in the A polyhedra.

In the present single-crystal structure analyses of $Ca_{1-x}Sr_xTiO_3$, we did not find superstructures such as those reported by Ball et al. (1998), Ranjan et al. (1999), and Leinenweber et al. (1997). Cation ordering at the A site may cause the superstructure. *Cmcm* symmetry in the orthorhombic region was proposed to result from a displacive phase transition (Ball et al. 1998) and shear strain (Carpenter et al. 2001). We did not recognize the presence of this phase in the possible region. Different sample preparations may cause this discrepancy. Single crystals of all samples used in the present experiment were synthesized by melt growth. Sample annealing at sufficiently low temperatures might give rise to superstructures through cation ordering.

The $SrTiO_3$ cubic phase ($Pm\bar{3}m$) is transformed to the tetragonal phase ($I4/mcm$) at 106 K (Ranjan et al. 1999) and $CaTiO_3$ shows the structure transition from orthorhombic ($Pbnm$) → tetragonal ($I4/mcm$) → cubic ($Pm\bar{3}m$) with increasing temperature (Redfern 1996; Liu and Liebermann 1993; Kennedy et al. 1999). These transitions are similar to our present experiments. However, the powder diffraction study of $CaTiO_3$ by Xiong et al. (1986) showed a hexagonal phase and a further cubic phase at elevated pressures. Their results are different from our high-pressure experiments and probably result from the nonhydrostatic conditions of their experiment. Metastable or unstable phases under nonhydrostatic conditions can be formed by slab dislocation induced from shear stress, which were seen in the $FeGeO_3$ polymorphic transformation under shear stress at 300 K: pyroxene → pseudoilmenite → ilmenite → perovskite under compression (Hattori et al. 2001).

On the contrary, with $BaTiO_3$ the structure symmetry is enhanced under high-pressure: orthorhombic → tetragonal → cubic perovskite (Minomura et al. 1964), which indicates a different sequence from those of $SrTiO_3$ and $CaTiO_3$. Hence the dP/dT curve is negative for $BaTiO_3$ and positive for $SrTiO_3$. In consideration of the structure change of $(Ca_{1-x}Sr_x)TiO_3$ in the present experiment, Figure 6 shows the structure type of $^{VIII}A^{2+VI}B^{4+}O_3$ perovskites under ambient conditions with reference to the previous studies. It is clearly seen in Figure 6 that the mutual relation between $^{VIII}A^{2+}$ and $^{VI}B^{4+}$ ionic radii defines the structure type and the possibilities for structural transitions. The ionic radii are taken from Shannon and Prewitt (1976). Our previous paper (Hattori et al. 1999) shows high-pressure perovskite polymorphs as a function of the tolerance factor t (= $(r_A + r_O)/\{\{\sqrt{2}(r_B + r_O)\}\}$). In general, since A^{2+} is more compressible than B^{4+}, t becomes smaller with compression. Hence perovskites with $t > 1$ at ambient pressure show a symmetry enhancement (e.g., $BaTiO_3$) under compression but those with $t < 1$ reduce their symmetry (e.g., $SrTiO_3$). ABO_3 compounds may yield different types of perovskite structures under high pressure; $CaSiO_3$ forms cubic perovskite but $MgSiO_3$ forms orthorhombic perovskite. Those having a larger A^{2+} cation than Ca^{2+} transform to cubic or pseudocubic perovskite under pressure. On the other hand, those with a smaller cation form orthorhombic perovskite at high pressure. The arrows in Figure 6 indicate the trend of structure changes or deformations at elevated pressure. Consequently the stable region for the orthorhombic phase in Figure 6 expands under high pressures. Orthorhombic $MgTiO_3$ or $MgSiO_3$ can be synthesized by application of pressure.

Homogeneous expansion or compression of the A and B cation sites, as found in $ScAlO_3$ (Yamanaka et al. 2000), does not necessarily result in a structure change. Generally, the tolerance factor is an indicator of the crystal symmetry of the perovskite structure, but the symmetry change of perovskites

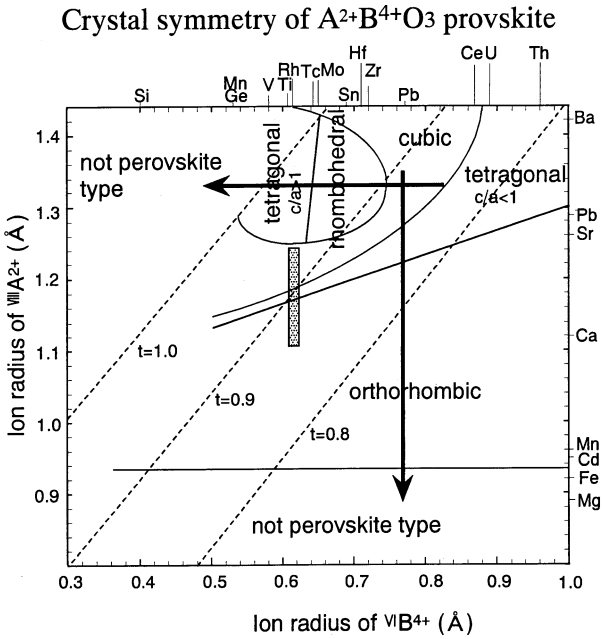

FIGURE 6. Structure type of $^{VIII}A^{2+VI}B^{4+}O3$ perovskites at ambient condition. $(Ca_{1-x}Sr_x)TiO_3$ perovskite is presented in the region between the orthorhombic and cubic structures.

The ionic radii are taken from Shannon and Prewitt (1976). The tolerance factors based on r_O = 1.40 Å for sixfold-coordinated O atoms are shown as a dashed line.

Arrows indicate the structure change or deformation at elevated pressure. Structures other than perovskite may form cubic ($CaSiO_3$), and orthorhombic ($MgSiO_3$) perovskites at high pressure.

with compression or heating is controlled by the mutual volume change of the A and B cation sites at high pressure and high temperature. Some perovskites become a higher symmetry phase at higher pressures and others show a lower symmetry. As can be seen from Figure 6, the inverse relationship between thermal change and pressure change is not always present in all perovskite structures.

REFERENCES CITED

Ball, C.J., Begg, B.D., Cookson, D.J., Thorogood, G.J., and Vance, E.R. (1998) Structures in the system $CaTiO_3/SrTiO_3$. Journal Solid State Chemistry, 139, 2328–247.

Bednorz, J.G. and Muller, K.A. (1984) An XY quantum ferroelecric with transition to randomness. Physical Review Letters, 52, 2289–2292.

Carpenter, M.A., Becerro, A.I., and Seifert, F. (2001) Strain analysis of phase transition in $(Ca,Sr)TiO_3$ perovskites. American Mineralogist, 86, 348–363.

Glazer, A.M. (1972) The classification of tilted octahedra in perovskite. Acta Crystallographica, B28, 3384–3392.

Hattori, T., Matsuda, T., Tsuchiya, T., Nagai, T., and Yamanaka, T. (1999) Clinopyroxene- perovskite phase transition of $FeGeO_3$ under high pressure and room temperature. Physics and Chemistry of Minerals, 26, 212–216.

Hattori, T., Tsuchiya, T., Nagai, T., and Yamanaka, T. (2001) Sequential high-pressure trans- formations of $FeGeO_3$ High-P clinopyroxene (C2/c) at temperatures up to 365 °C. Physics and Chemistry of Minerals, 28, 377–387.

Hayward, S.A. and Salje, E.K.H. (1999) Cubic-tetragonal phase transition in $SrTiO_3$ revised: Landau theory and transition mechanism. Phase Transitions, 68, 501–522.

Howard, C.J. and Stokes, H.T. (1998) Group-theoretical analysis of octahedral tilting in perovskite. Acta Crystallographica, B54, 782–789.

Horiuchi, H., Ito, E., and Weidner, D.J. (1987) Perovskite-type $MgSiO_3$: Single crystal x-ray diffraction study. American Mineralogist, 72, 357–360.

Kennedy, B.J., Howard, C.J., and Chakoumakos, B.C. (1999) Phase transitions in perovskite at elevated temperatures—a powder neutron diffraction study. Journal of Physics Condensed Matter, 11, 1479–1488.

Leinenweber, K., Grzechnik, A., Voorhees, M., Navrotsky, A., Yao, A., and McMillan, P.F. (1997) Structure variation in $Ca(Ti_xSi_{1-x})O_3$ perovskite ($1 > x > 0.65$) and ordered phase Ca_2TiSiO_6. Physics and Chemistry of Minerals, 24, 528–534.

Liu, X. and Liebermann, R.C. (1993) X-ray powder diffraction study of $CaTiO_3$ perovskite at high temperature. Physics and Chemistry of Minerals, 20, 171–173.

Mao, H.K., Hemley, C.R., Jephcoat, A.P., and Wu, Y. (1989) Stability and Equation of state of $CaSiO_3$-perovskite to 134 GPa. Journal of Geophysical Research, 94, 17,889–17,894.

Minomura, S., Kawakubo, Nakagawa, T., and Sawada, S. (1964) Pressure dependence of Curie point and tetragonal-orthorhombic transition point of $BaTiO_3$. Japan Journal Applied Physics, 3, 562–563.

Ranjan, R., Pandey, D., Siruguri, V., Krishna, P.S.R., and Paranjpe, S.K. (1999) Novel structure features and phase transition behavior of $(Sr_{1-x}Ca_x)TiO_3$: I. Neutron diffraction study. Journal of Physics: Condensed Matter, 11, 2233–2246.

Redfern, S.A.T. (1996) High-temperature structural phase transitions in perovskite ($CaTiO_3$). Journal of Physics: Condensed Matter, 8, 8267–8275.

Ross, N.L. and Angel, R.J. (1999) Compression of $CaTiO_3$ and $CaGeO_3$ perovskites. American Mineralogist, 84, 277–281.

Salje, E.K.H., Gallardo, M.C., Jumenez, J., Romero, F.J., and del Cerro, J. (1998) The cubic- tetragonal phase transition in strontium titanate: excess specific heat measurements and evidence for a near tricritical mean field type transition mechanism. Journal of Physics Condensed Matter, 10, 5535–5543.

Sasaki, S., Prewitt, C.T., and Bass, J. (1987) Orthorhombic perovskite $CaTiO_3$ and $CdTiO_3$: structure and space group. Acta Crystallographica, C43, 1668–1674.

Shannon, R.D. and Prewitt, C.T. (1976) Revised effective ionic radii and systematic studies of interatomic distances in halide and chalcogenides. Acta Crystallographica, A32, 751–767.

Shim, S.H., Duffy, T.S., and Shen, G. (2000a) The equation of state of $CaSiO_3$ perovskite to 108 GPa at 300 K. Physics of Earth Planetary Interiors, 120, 327–338.

———(2000b) The stability and P-V-T equation of state at $CaSiO_3$ perovskite in the Earth's lower mantle. Journal of Geophysical Research, 105, 25,955–25,968.

Tokonami, M. (1965) Atomic scattering factor for O^{-2}. Acta Crystallographica, 19, 486–488.

Wang, Y., Weidner, D.J., and Guyot, F. (1996) Thermal equation of state of $CaSiO_3$ perovskite. Journal of Geophysical Research, 101, 661–672.

Wilson, A.J.C. (1992) International Tables of Crystallography C, 477–498, Kluwer Acadmic Publisher, London.

Xiong, D.H., Ming, L.C. and Manghnani, M.H. (1986) High-pressure phase transformation and isothermal compression in $CaTiO_3$ (perovskite). Physics of Earth Planetary Interiors, 43, 244–252.

Yagi, T., Kusanagi, S., Tsuchida, Y., and Fukai, Y. (1989) Isothermal compression and stability of perovskite $CaSiO_3$. Proceeding of Japan Academy of Science, 65, 129–132.

Yamanaka, T., Lieberman, R.C., and Prewitt, C.T. (2000) Thermal expansion of aluminus perovskite $ScAlO_3$. Journal of Mineralogical and Petrological Sciences, 95, 182–192.

Yamanaka, T., Fukuda, T., Hattori, T., and Sumiya, H. (2001) New Diamond anvil cell for single-crystal analysis. Review of Scientific Instruments, 72, 1456–1462.

MANUSCRIPT RECEIVED SEPTEMBER 17, 2001
MANUSCRIPT ACCEPTED APRIL 24, 2002
MANUSCRIPT HANDLED BY YINGWEI FEI